Production, Characterization, and Scattering of a Beam of Sulfur Monoxide Radicals: The SO−Noble Gas Interactions

Vincenzo Aquilanti,*,† Daniela Ascenzi,† Elisabetta Braca,† David Cappelletti,‡ Giorgio Liuti,‡ Emilio Luzzatti,† and Fernando Pirani†

Dipartimento di Chimica dell'Università, Universita di Perugia, I-06123 Perugia, Italy, and Facoltà di Ingegneria, Istituto per le Tecnologie Chimiche, I-06123 Perugia, Italy

Received: March 4, 1997; In Final Form: April 25, 1997[⊗]

An intense and stable continuous beam of SO radicals has been produced with a microwave-discharge source operating in the Torr range in mixtures of SO_2 with various gases. The free-radical beam emerging from the plasma source is velocity analyzed by a mechanical velocity selector and detected by a quadrupole mass filter. Stern−Gerlach magnetic analysis shows SO radicals mainly in the electronic ground state $^3\Sigma^-$ with a rotationally hot distribution and provides an upper limit ($\leq$7%) on the concentration of electronic metastable states. Total integral cross-section measurements as a function of velocity in the range 0.9−2.4 km·s^{-1} for the scattering of ground-state SO radicals by Ne, Ar, and Kr have also been performed. The analysis of experimental data (cross sections and their velocity dependence, which exhibits glory interference patterns) allows a characterization of the interaction potential features for the investigated systems. Use of a correlation rule leads to an estimate of the average polarizability of the SO molecule and also of the potential features for SO−He and SO−Xe.

1. Introduction

The production of intense and stable beams of open-shell atoms and free radicals is crucial for the study of many elementary physicochemical phenomena. Scattering experiments of open-shell species by closed-shell atoms and molecules are relevant for the experimental characterization of the weak interactions which typically drive gas-phase collisions. The understanding of the nature of these interactions, weaker than chemical bonds but, in some cases, stronger than pure van der Waals intermolecular forces, is of interest for assessing the selective role of long-range forces in determining the outcome of elastic and inelastic events, as well as of reactive processes.

This paper presents some investigations on the production, characterization, and use for scattering measurements of a beam of SO radicals, obtained by dissociating SO_2 molecules in a microwave discharge. Recent investigations have focused on the study of SO production from vacuum UV photolysis of SO_2[1,2] and other molecules.[1,3−5]

Physicochemical properties of SO radicals are of considerable interest for a variety of processes concerning many diverse areas such as upper planetary atmospheres[6] and interstellar molecular clouds,[7] combustion,[8] and air pollution reactions.[9] Moreover, the SO radicals are important reaction intermediates[10] and play a role in the Earth's sulfur cycle.[11]

Similarly to its isovalent species, O_2, the SO radical shows three electronic states that can be populated in microwave plasmas: the electronic ground $X^3\Sigma^-$ intermediate between Hund's a and b coupling schemes[12,13] is paramagnetic; the first low-lying (energy ∼0.79 eV above ground) metastable excited state $a^1\Delta$, belonging to Hund's case a, presents a paramagnetism which decreases at high rotational temperature; finally, the second excited state $b^1\Sigma^+$ (energy 1.303 eV) is diamagnetic at all rotational temperatures. These particular magnetic properties will be exploited in a Stern−Gerlach analysis to establish that the concentration of metastable state in the beam is low enough to allow us to perform collision studies in order to characterize the interactions of ground-state SO radicals.

The experimental apparatus and the magnetic analysis technique are illustrated in sections 2 and 3. Scattering experiments are described in section 4, and the analysis of the obtained total integral cross sections is described in section 5. Conclusions will follow in section 6.

2. Experimental Setup

In recent years, several systems, concerning ground-state open-shell atoms such as oxygen,[14] fluorine,[15] and chlorine,[16] have been investigated by us through scattering studies carried out with magnetically analyzed atomic beams.[17,18] The magnetic analysis technique is used to obtain the atomic sublevel populations in the beam and to change their values in a controlled way.

The present experimental apparatus, schematized in Figure 1, is essentially the same as used before. It consists of a set of several differentially pumped vacuum chambers where the beam, produced in a discharge source, to be described later, is mechanically velocity selected (5% FWHM) by rotating slotted disks, is then magnetically analyzed by a Stern−Gerlach magnet in Rabi configuration, and detected by electron bombardment ionization and quadrupole mass spectrometry. Only those details specifically relevant for the production, characterization, and detection of the SO radical beam will be given in the following.

The beam source consists of a quartz cell, confined inside a near-resonant microwave cavity operated at 2450 MHz and a nominal power of approximatively 100 W. The SO radicals were produced by discharge in SO_2, both pure and in mixtures with various gases (Ar, N_2, O_2, He). Optimal yield, beam intensity sufficiently high in a wide velocity range, and minimal interference in the mass spectrum at $m/e = 48$ were obtained with a microwave plasma generated in a 1:1 He:SO_2 gaseous mixture at a total pressure of ∼4 Torr.

The mass spectrometric analysis has revealed a high concentration of SO radical in the beam and also the presence of

† Universita di Perugia.
‡ Istituto per le Tecnologie Chimiche.
⊗ Abstract published in *Advance ACS Abstracts,* July 1, 1997.

S1089-5639(97)00817-7 CCC: $14.00

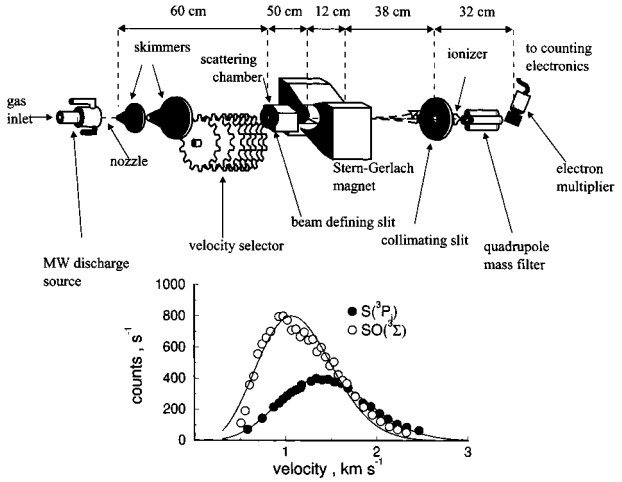

Figure 1. Experimental apparatus for magnetic analysis and total integral cross-section measurements (in the drawing, not all the distances are to scale). In the panel, velocity distributions of the SO radicals and S atoms produced in the microwave-discharge source are reported, giving also indicative numbers for the counting rates. The solid curves are the best-fit calculations assuming near Boltzmann distributions at source temperatures $T_0 \simeq 2000$ K and final translational temperatures $T_f \simeq 1500$ K for both species.

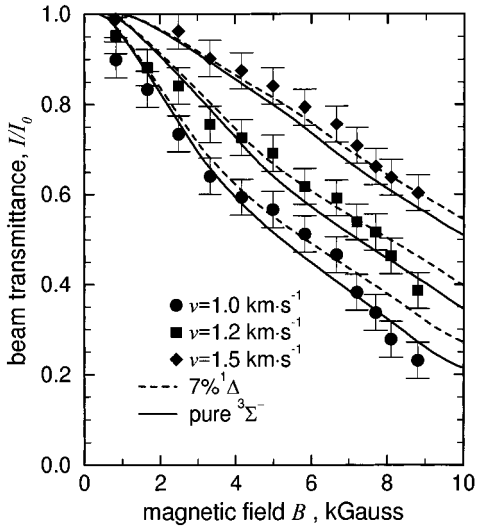

Figure 2. Beam transmittance I/I_0 for the SO radical measured as a function of the magnetic field B at three different selected beam velocities v. Solid lines are calculations assuming the exclusive population of the $^3\Sigma^-$ state at a rotational temperature $T = 1500$ K; dashed lines are the best-fit calculations performed adding a fraction of 0.07 of $^1\Delta$ state at the same rotational temperature.

S atoms and higher mass species, containing S and O atoms, produced in the plasma. Under the present typical operative conditions, the estimated dissociation percentage of the SO_2 precursor is about 50% and the velocity distributions for the SO and S species, formed approximatively in a 2:1 ratio (see Figure 1 for indicative counting numbers), appear to be sufficiently broad to enable magnetic analysis and scattering experiments to be performed in a wide energy range. Since the higher mass species showed a large contribution from the parent ion fragmentation in the lower tail of the velocity spectrum of both SO and S, all the scattering experiments were performed at collision energies high enough to exclude such a contamination and, in particular, above the peak velocity ($v \geq 1.0$ km·s^{-1}) of the SO radical beam.

In the third chamber, after a path of ~60 cm from the source, the beam passes through a defining slit of 0.35 mm in radius and then crosses the scattering chamber. This copper-made chamber can be cooled to 80−90 K in order to decrease the thermal motion of the target gas, typically kept at a pressure range between 10^{-2} and 10^{-3} Torr. The detector housing is maintained under ultrahigh-vacuum conditions (~10^{-10} Torr).

Figure 1 shows arrangements and typical distances along the beam path. The distance between the beam-defining slit before the scattering chamber and the ionization zone in the detector (100 cm), together with the radius of the slit, determines the angular resolution of the apparatus θ_r at 5×10^{-4} rad, estimated according to ref.[19] This angle is needed to evaluate the possible systematic errors in the measured integral cross section which are expected to increase when fast and heavy projectiles collide with heavy targets. The inherent "error" u in the cross section, due to the finite angular resolution,[20] can be calculated from

$$u = \frac{1}{2}(\theta_r/\theta^*)^2 \qquad (1)$$

where θ^* is the limiting angle given by

$$\theta^* = (\hbar/\mu v)(2\pi/Q)^{1/2} \qquad (2)$$

Here, μ is the reduced mass of the colliding partners, v is the relative velocity, and Q is the integral cross section at the same velocity (see section 4). The use of the above equations will be shown in section 4 to lead to corrections negligible for SO−Ne, small for SO−Ar, and large for SO−Kr.

3. Characterization of the Beam by Magnetic Analysis

Since the SO radical beam is produced from a microwave discharge in a He−SO_2 mixture, it is worthwhile to assess the role of possible metastable electronic states. In fact, as in the similar case of the O_2 molecule,[21] not only the ground $^3\Sigma^-$ but also the excited and long-lived metastable $^1\Delta$ and $^1\Sigma^+$ states can be expected to be populated in a microwave plasma. Their lifetimes, ~450[22] and ~6 ms,[23] respectively, are sufficiently long for them to survive during the flight time in the apparatus (less than 1 ms).

As before,[17,18,21] the characterization of a beam containing paramagnetic species is performed in the transmission mode with the Stern−Gerlach magnetic selector inserted along the beam path and located, in the present experiments, 110 cm from the source nozzle (see Figure 1). The beam transmittance I/I_0, defined as the ratio between the beam intensity with and without magnetic field, has been measured as a function of the applied magnetic field and at beam velocities of 1.0, 1.2, and 1.5 km·s^{-1} (see Figure 2).

The action of an inhomogeneous magnetic field on a beam composed of paramagnetic species of the same mass and velocity is to induce different deflections depending on the values of the effective magnetic moments of the various particles. For a species in a defined quantum state i, to which a potential energy E_i is associated as a function of an external magnetic field strength B, the effective magnetic moment μ_i is given by

$$\mu_i = -\frac{\partial E_i}{\partial B} \qquad (3)$$

Accordingly, the measured beam transmittance, which is determined by the effective magnetic moments, is strongly dependent on the features of the populated quantum states i.

The next question is the determination of the dependence of E_i on B. As mentioned above, the angular momentum coupling for SO in the electronic state $^3\Sigma^-$ is close to a pure Hund's case (b). In this case, the rotational **K** and electron spin **S** (S

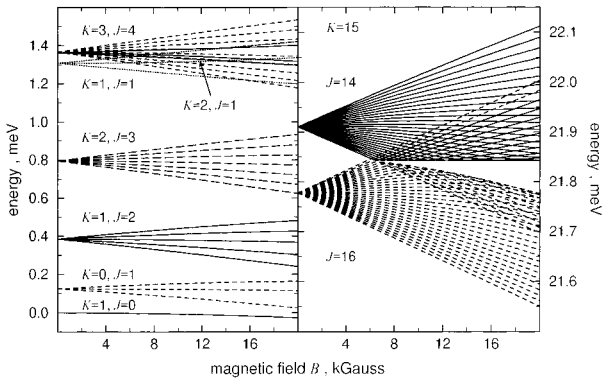

Figure 3. Zeeman energy levels as a function of the magnetic field *B*: in the left panel, the lowest *K*, *J* spin rotation levels are reported; in the right panel, the case of a high-*K* level is exemplified by $K = 15$, $J = 14$; $J = 16$ spin rotational levels.

$= 1$) angular momenta are coupled to produce the total angular momentum $\mathbf{J} = \mathbf{K} + \mathbf{S}$. Therefore, the resulting *J* can only have three values for each *K* level, $K + 1$, *K*, and $K - 1$, which correspond to different spin−rotational levels. The high value of the spin−rotation coupling constant of SO, $^3\Sigma^-$, generates a peculiar fine structure which shows two features relevant for the present analysis:

(1) For low *K* values ($K < 5$, involved energies lower than 3.4 meV), the spin−rotational levels appear to be more separated than the rotational states (see Figure 3 for low-lying states).

(2) In the magnetic field range of our experiments, as the external field *B* increases up to a maximum of about 10 kG, there is only a progressive partial decoupling between **K** and **S**, since a full Paschen−Back effect (**K** and **S** independently coupled to **B**) occurs at *B* values of the order of magnitude of 10^2 kG. As a consequence, each fine structure component *J* has $2J + 1$ sublevels resulting from the possible different orientations of **J** around the magnetic field direction, which are defined by the quantum number m_J.

In the past, the analysis of the observed electron paramagnetic spectrum of sulfur monoxide[24,25] was made using a Hamiltonian, appropriate for the $^3\Sigma^-$ molecule and originally derived by Tinkham and Strandberg in their study of molecular oxygen,[26] which contains fine structure and magnetic-field-dependent terms. The basis sets for which the Hamiltonian matrix can be written in simple forms are those in which the angular momentum coupling is exactly either Hund's case *a* or Hund's case b. The complete description of the matrix elements for SO in a case *b* basis set is reported in ref.[24] These elements depend on the magnetic field strength and are functions of the coupling constants and quantum numbers *J* and m_J. Here, we use the same values of the coupling constants for SO molecules as those given in refs.[27] Numerical diagonalization of the secular equation leads to the Zeeman levels E_{K,J,m_J} as a function of the magnetic field *B*. Some results are shown in Figure 3 for two different cases: the first is with regard to rotational levels $K = 0$, 1, 2 for which the spin−rotational interaction overcomes separation of rotational levels; the second refers to a high *K* value, specifically $K = 15$ ($J = 14$ and 16).

The derivatives of the Zeeman energy levels, as a function of *B*, give the magnetic moments values, useful for the present analysis. Beam transmittances I/I_0, for SO molecules in the electronic ground state $^3\Sigma^-$, are computed as discussed elsewhere[17,21] and assuming a Boltzmann distribution of the spin−rotational levels corresponding to various temperatures *T*. The I/I_0 behavior as a function of magnetic field strength *B*, at sufficiently high *T* values typical of hot and near-effusive beams, is almost independent from assumed *T* values (as already observed for the O_2 case[21]). In the present experiment, a lower limit for *T* (∼1500 K) can be estimated from the final translational temperature T_f, determined through the velocity analysis; see Figure 1.

The molecular beam transmittances so calculated for the three selected beam velocities show a substantial agreement with experimental data (see Figure 2), and this suggests that the produced SO beam is mainly formed by molecules in the electronic ground state. Nevertheless, an estimate for the upper limit of the metastable states concentration in the beam can be given. To this purpose, we can neglect any contribution from the diamagnetic $^1\Sigma^+$ state and take into account only possible effects from the $^1\Delta$ state. For the latter, the first-order effective magnetic moment μ_{J,m_J} can be obtained from available Zeeman level formulas:[13]

$$\mu_{J,m_J} = \frac{4g_L\mu_0 m_J}{J(J+1)} \tag{4}$$

where $g_L \simeq 1$ and μ_0 is the Bohr magneton. Since this state is a pure Hund's case *a*, the values of the total angular momentum are $J = 2$, 3, 4, ..., and paramagnetism is seen to decrease rapidly as *J* increases. Assuming the presence in the beam of a fraction *c* of SO radicals in the $^1\Delta$ state, the beam transmittance is given by

$$\frac{I}{I_0} = (1-c)\left(\frac{I}{I_0}\right)_{^3\Sigma^-} + c\left(\frac{I}{I_0}\right)_{^1\Delta} \tag{5}$$

An upper limit for *c* corresponding to 0.07 can be obtained by using a *J* distribution associated to a spin−rotational temperature $T = 1500$ K. The beam transmittances so calculated are compared with those computed in the case of SO in a pure $^3\Sigma^-$ state and with the experimental results in Figure 2.

4. Total Integral Cross-Section Measurements: Data Analysis and Interaction Potentials

It is well-established from thermal energy elastic-scattering studies of atom−atom collisions[28] that integral cross sections may exhibit, as a function of the collision velocity v, an oscillatory behavior (glory effect) superimposed over a monotonic trend. Typically, the latter, which probes the long-range part of the interaction, decreases as $v^{-2/5}$ and is mainly responsible for the size of the cross section. The glory undulations arise from the interference between two types of trajectories, both leading to no net deflection: the first type corresponds to trajectories at small impact parameters, for which the attractive and repulsive actions balance; the second type is due to collisions at impact parameters so large that the effect of the potential is negligible. Amplitudes and frequencies of these undulations are connected to features of the potential, such as the depth of the well ϵ and its location R_m.

The absolute total cross section $Q(v)$ for the scattering of the SO radicals on Ne, Ar, and Kr, measured as a function of the beam velocity v, are reported in Figure 4 and are plotted as $Q(v)v^{2/5}$ to emphasize the observed glory interference pattern.

Because of the high SO rotational temperature, a substantially isotropic interaction can be expected in the SO−noble gases collisions. Therefore, a single spherical potential model can be used for the analysis of the experimental data for all three investigated systems. As usual, we employ a MSV (Morse−spline−van der Waals) parameterization for the interaction potential (see below) and standard computation techniques[29] for cross-section calculations. The total cross sections calculated in the center-of-mass frame are convoluted in the laboratory system,[30] considering the thermal motion of the target gas, the

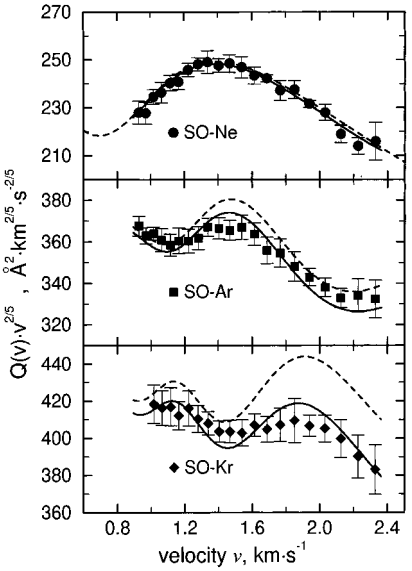

Figure 4. Absolute total cross sections $Q(v)$ for the SO−Ne, Ar, and Kr systems, as a function of the beam velocity v and plotted as $Q(v)v^{2/5}$ to emphasize the glory interference pattern. Dashed lines are calculations for the true quantum cross sections Q_{tr} in the laboratory system; solid lines are calculations corrected to take into account the finite angular resolution of the experimental apparatus, as explained in the text.

transmission function of the mechanical velocity selector, and the finite angular resolution of the apparatus. They are plotted as solid lines in Figure 4, for a comparison with those experimentally measured.

The effect of the finite angular resolution of the experiment produces a lowering in the absolute value of the cross sections, which influences also the amplitude of the observed interference glory structure. This effect, as discussed in section 2, depends critically on the reduced mass of the systems and increases with the collision energy. As a result, the measured integral cross section Q is given by[20]

$$Q = Q_{tr} - uQ_{tr} \tag{6}$$

where Q_{tr} represents the true cross section and u is the "error" due to the finite angular resolution of the apparatus defined in eq 1.

In Figure 4, dashed lines represent the true quantum cross section calculated in the laboratory frame using the best-fit parameters listed below, while solid lines take into account the proper correction due to the finite angular resolution of the apparatus. This effect is negligible in SO−Ne; it is detectable in SO−Ar and appears to be more evident in the SO−Kr case. Since the effect would have been more severe for the SO−Xe system, we did not extend the present investigation to include the Xe case. In the case of SO−He, the angular resolution correction would also be negligible. However, we did not perform scattering measurements for the helium system because the glory structure is outside the experimentally accessible collision velocity range.

Figure 4 also illustrates that the calculated glory extrema with the proper correction are still well observable in all systems and their amplitude is in agreement with the experimental findings. This is a confirmation[31] that in the case of a molecular beam effusing from a source at high temperature, the rotational interaction anisotropy, although present in all cases, affects only slightly the glory oscillations. In addition, the amplitude of the oscillations suggests that the metastable states, present in low concentration in the beam, do not affect sensibly the present measurements.

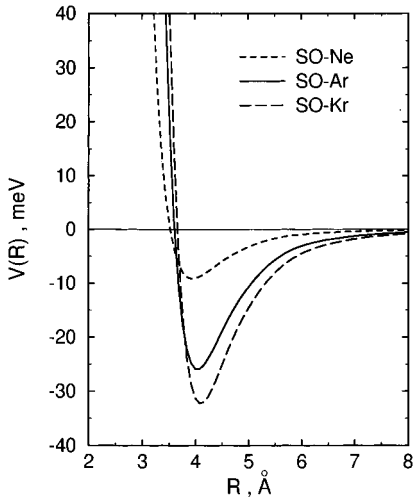

Figure 5. Potential energy curves for the SO−Ne, Ar, and Kr systems.

The best-fit potential curves are shown in Figure 5. The functional form of the potential according to the MSV parameterization, which can be expressed as scaling for location R_m and depth ϵ of the potential well,

$$x = \frac{R}{R_m} \qquad f(x) = \frac{V_0(R)}{\epsilon} \tag{7}$$

is the following:

Morse

$$f(x) = \exp[-2\beta(R/R_m - 1)] - 2\exp[-\beta(R/R_m - 1)] \quad \text{for} \quad x \le x_1 \tag{8}$$

spline

$$f(x) = b_1 + (x - x_1)b_2 + (x - x_2)[b_3 + (x - x_1)b_4] \quad \text{for} \quad x_1 < x < x_2 \tag{9}$$

van der Waals

$$f(x) = -\left(\frac{C_6}{\epsilon R_m^{\,6}}\right)x^{-6} \qquad \text{for} \quad x \ge x_2 \tag{10}$$

The β parameter, which defines the well shape of the potential, is fixed at 6.5, a value which is characteristic of van der Waals forces;[32] x_1 and x_2 are chosen, as for other previous cases,[15] in the neighborhood of 1.1 and 1.5, while b_1, b_2, b_3, and b_4—the spline parameters—are automatically fixed by imposing that the functions must have the same value and the same derivative at x_1 and x_2. The analysis of the smooth component (i.e., $\simeq v^{-2/5}$) of the cross-section dependence on velocity gives direct information on the long-range effective interaction constants C_6, while, from the glory patterns, the well depth ϵ and location R_m are obtained by a trial-and-error procedure.

The values of the relevant parameters are reported in Table 1 for all the investigated systems together with the estimated experimental uncertainties.

5. Final Remarks and Conclusions

A microwave-discharge source has been used to produce a beam of SO radicals from an SO_2:He mixture. The free-radical beam has been characterized by means of velocity and magnetic selection techniques. The analysis of the electronic and

TABLE 1: Potential Parameters, As Determined Experimentally, for SO ($X^3\Sigma^-$) Interacting with Ne, Ar, and Kr[a]

	R_m, Å	ϵ, meV	C_6, meV Å^6
SO−He	*3.84*	*2.7*	*1.2 × 10^4*
SO−Ne	3.95	5.7	2.5 × 10^4
SO−Ar	4.04	16.2	8.9 × 10^4
SO−Kr	4.10	20.1	1.3 × 10^5
SO−Xe	*4.27*	*22.8*	*1.9 × 10^4*

[a] The estimated uncertainties are ∼10% for the well depth ϵ and long-range constant C_6 and ∼2% for the well location R_m, except for the C_6 of SO−Kr system where the uncertainty is ∼15%. Also reported, in italics, are the estimated quantities (see text) for the SO−He and SO−Xe interaction pairs: in these cases, uncertainties can be taken as ∼15% for the well depth ϵ and long-range constant C_6 and ∼3% for the well location R_m.

rotational state distributions revealed that a large fraction of the radicals are produced in the ground $^3\Sigma^-$ electronic state with a rotational temperature ≥ 1500 K. Total integral cross-section measurements for the scattering of ground-state SO radicals by Ne, Ar, and Kr have also been performed.

The analysis of the scattering data has allowed a characterization of the interaction potential features for the investigated systems (see Table 1). It is interesting to note how the obtained bond energies ϵ increase from SO−Ne toward SO−Kr, while the bond lengths R_m are nearly the same for all systems. This behavior is typical of van der Waals systems, when the same highly polarizable particle, the SO radical in this case, interacts with different and less polarizable partners.[33] Actually, it is possible to extract information on the average polarizability α of the SO radical in the ground $^3\Sigma^-$, from the experimentally measured potential parameters ϵ, R_m, and C_6. This can be done using well-established correlation formulas[33] between the potential parameters and the polarizability of interacting partners, as already done in the case of N_2 in the first excited $^3\Sigma_u^+$ state.[34]

The comparison of the mentioned formulas with the ϵ, R_m, and C_6 values experimentally determined yield a value of 3.5 ± 0.3 Å^3 for the average polarizability of SO. For the calculation of C_6, an effective electron number[33] of 10.2 has been used for the SO species. It is to be noted that the value of α so obtained is equal or slightly lower than the sum of the polarizabilities of the separated atoms in their ground states (for the S atom, α = 2.9 Å^3; for the O atom, α = 0.8 Å^3).

The features of the interaction of the SO−He and SO−Xe systems have not been determined experimentally, because they are not accurately investigable with the present settings of the apparatus. In particular, for the helium case, the glory region is located at lower energies with respect to the ones experimentally accessible, while the angular resolution of the apparatus is insufficient to avoid strong limit angle effects (see eqs 1 and 2) induced by the high mass and large cross section of xenon. Nevertheless, an estimate of the main interaction parameters for the SO−He and SO−Xe systems can be done with the application of the abovecited correlation formulas and with the use of the determined value of the polarizability of the SO radical. The results (together with the estimated uncertainties) are reported in Table 1.

Acknowledgment. This work is supported by the Italian National Research Council (CNR), by the Ministero dell'Università e della Ricerca Scientifica e Tecnologica (MURST), and by the European Union within the Human Capital and Mobility Network "Structure and Reactivity of Molecular Ions" (Contract No. CHRX-CT93-0150), the Training and Mobility of Researchers Network "Potential Energy Surfaces for Molecular Spectroscopy and Dynamics" (Contract No. ERB-FMRX-CT96-0088), and the COST D-3 action.

References and Notes

(1) Chen, X.; Asmar, F.; Wang, H.; Weiner, B. R. *J. Phys. Chem.* **1991**, *95*, 6415.
(2) Stuart, B. C.; Cameron, S. M.; Powell, H. T. *J. Phys. Chem.* **1994**, *98*, 11499.
(3) Chen, X.; Wang, H.; Weiner, B. R. *J. Phys. Chem.* **1993**, *97*, 12269.
(4) Zhao, H.-Q.; Cheung, Y.-S.; Heck, D. P.; Ng, C. Y.; Tetzlaff, T.; Jenks, W. S. *J. Chem. Phys.* **1997**, *106*, 86.
(5) Blank, D. A.; North, S. W.; Stranges, D.; Suits, A. G.; Lee, Y. T. *J. Chem. Phys.* **1997**, *106*, 539.
(6) Lellouch, E.; Strobel, D. F.; Belton, M. J. S.; Summers, M. E.; Paubert, G.; Moreno, R. *Astrophys. J.* **1996**, *459* (2, Part 2), L107. Na, C. Y.; Esposito, L. W.; McClintock, W. E.; Barth, C. A. *Icarus* **1994**, *112*, 389. Moses, J. I.; Allen, M.; Gladstone, G. R. *Geophys. Res. Lett.* **1995**, *22*, 1601.
(7) Turner, B. E. *Astrophys.J.* **1995**, *455* (2, Part 1), 556.
(8) Woiki, D.; Roth, P. *Int. J. Chem. Kinet.* **1995**, *27*, 59. Tyndall, G. S.; Ravishankara, A. R. *Int. J. Chem. Kinet.* **1991**, *23*, 483.
(9) Brunning, J.; Stief, L. J. *J. Chem. Phys.* **1986**, *84*, 4371. Brunning, J.; Stief, L. J. *J. Chem. Phys.* **1986**, *85*, 2591.
(10) Smardzewski, M. M.; Lin, M. C. *J. Chem. Phys.* **1977**, *69*, 3197. Tevault, D. E.; Smardzewski, M. M. *J. Chem. Phys.* **1978**, *69*, 3182.
(11) DeMore, W. B.; Yung, Y. L. *Science* **1982**, *217*, 1209.
(12) Clark, W. W.; De Lucia, F. C. *J. Mol. Spectrosc.* **1976**, *60*, 332.
(13) Herzberg, G. Molecular Spectra and Molecular Structure, *Spectra of Diatomic Molecules*; Van Nostrand: Princeton, NJ, 1967; Vol. 1, p 301.
(14) Aquilanti, V.; Candori, R.; Mariani, L.; Pirani, F.; Liuti, G. *J. Phys. Chem.* **1989**, *93*, 130.
(15) Aquilanti, V.; Candori, R.; Cappelletti, D.; Luzzatti, E.; Pirani, F. *Chem. Phys.* **1990**, *145*, 293.
(16) Aquilanti, V.; Cappelletti, D.; Lorent, V.; Luzzatti, E.; Pirani, F. *J. Phys. Chem.* **1993**, 97, 2063. Aquilanti, V.; Cappelletti, D.; Pirani, F. *J. Chem. Soc., Faraday Trans.* **1993**, *89*, 1467.
(17) Aquilanti, V.; Candori, R.; Cappelletti, D.; Lorent, V.; Pirani, F. *Chem. Phys. Lett.* **1992**, *192*, 145.
(18) Aquilanti, V.; Ascenzi, D.; Cappelletti, D.; Pirani, F. *J. Chin. Chem. Soc.* **1995**, *42* 263.
(19) Kusch, P. *J. Chem. Phys.* **1964**, *40*, 1.
(20) Dehmer, P.; Wharton, L. *J. Chem. Phys.* **1972**, *57*, 4821.
(21) Aquilanti, V.; Ascenzi, D.; Cappelletti, D.; Pirani, F. *Int. J. Mass Spectrosc. Ion Process.* **1995**, *149/150*, 355.
(22) Klotz, R.; Marian, C. M.; Peyerimhoff, S. D.; Hess, B. A.; Buenker, R. J. *Chem. Phys.* **1984**, *89*, 223.
(23) Wildt, J.; Fink, E. H.; Winter, R.; Zabel, F. *Chem. Phys.* **1983**, *80*, 167.
(24) Carrington, A.; Levy, D. H.; Miller, T. A. *Proc. R. Soc. London, Ser. A* **1967**, *298*, 340.
(25) Daniels, J. M.; Dorain, P. B. *J. Chem. Phys.* **1966**, *45*, 26.
(26) Tinkham, M.; Strandberg, M. W. P. *Phys. Rev.* **1955**, *97*, 937; **1955**, *97*, 951.
(27) Tiemann, E. *J. Mol. Spectrosc.* **1982**, *91*, 60. Davies, P. B.; Wayne, F. D.; Stone, A. J. *Mol. Phys.* **1974**, *28*, 1409. Cazzoli, G.; Cludi, L.; Cotti, G.; Degli Esposti, C.; Dore, L. *J. Mol. Spectrosc.* **1994**, *167*, 468.
(28) Bernstein, R. B.; O'Brien, T. J. P. *Discuss. Faraday Soc.* **1965**, *40*, 35. Bernstein, R. B.; O'Brien, T. J. P. *J. Chem. Phys.* **1967**, *46*, 1208.
(29) Pirani, F.; Vecchiocattivi, F. *Mol. Phys.* **1982**, *45*, 1003.
(30) Liuti, G.; Luzzatti, E.; Pirani, F.; Volpi, G. G. *Chem. Phys. Lett.* **1987**, *135*, 387.
(31) Aquilanti, V.; Beneventi, L.; Grossi G.; Vecchiocattivi, F. *J. Chem. Phys.* **1988**, *89*, 751.
(32) Aquilanti, V.; Cappelletti, D.; Pirani, F. *Chem. Phys.* **1996**, *209*, 299.
(33) Cambi, R.; Cappelletti, D.; Liuti, G.; Pirani, F. *J. Chem. Phys.* **1991**, *95*, 1852.
(34) Cappelletti, D.; Liuti, G.; Pirani, F. *J. Chem. Phys.* **1994**, *101*, 1225.